

Characterization of an experimental turbulent vortex in the physical and spectral spaces

YANNIS CUYPERS[†], AGNÈS MAUREL[‡] and PHILIPPE PETITJEANS[†]

[†]Laboratoire de Physique et Mécanique des Milieux Hétérogènes, UMR CNRS 7636, Ecole Supérieure de Physique et de Chimie Industrielles, 10 rue Vauquelin, 75005 Paris, France
[‡]Laboratoire Ondes et Acoustique, UMR CNRS 7587, Ecole Supérieure de Physique et de Chimie Industrielles, 10 rue Vauquelin, 75005 Paris, France

We present an experiment where a stretched vortex is experiencing quasi-periodical turbulent bursts inside a laminar environment. In previous studies (Cuypers *et al.*, 2003 *Phys. Rev. Lett.*, **91**, 194502, Cuypers *et al.*, 2004 *J. Turb.*, **5**), the classical $k^{-5/3}$ decay of the spectrum resulting from the evolution of this burst has been characterized and interpreted in the framework of Lundgren's mechanism (Lundgren 1982 *Phys. Fluids* **25** 2193). In this paper, the flow is further characterized in both the physical and the spectral spaces using a statistical exploitation of phase averaged particle image velocimetry measurements.

1. Introduction

In previous studies [1, 2], the authors have shown that the studied flow, i.e. the turbulence resulting from the quasi-periodical burst of a stretched vortex inside a laminar environment was responsible for the build-up of a Kolmogorov $k^{-5/3}$ energy spectrum. The construction of this spectrum with time has been studied. It has been shown that the $-5/3$ exponent results from the time-averaged contribution of the turbulent burst over its typical evolution time $T_v \approx 1.5$ s. Instantaneously, the energy spectra exponents have been shown to follow a transition between -1 and -2 over T_v .

The results have been compared and interpreted with the Lundgren stretched spiral vortex model [3] that shows some common features with the experimental flow. The Lundgren vortex is an asymptotic solution of the Navier-Stokes equation exhibiting an energy cascade mechanism resulting from a single structure evolution. This mechanism results from the evolution of the non-axisymmetric vorticity part of the structure under the influence of two ingredients: the uniform stretching imposed to the structure and its own differential rotation. In the Lundgren vortex model, the initial vorticity field is a free parameter for which the only constraint is the presence of a differential rotation. Different choices for the initial vorticity field yield different spiral structures and finally different instantaneous spectra. As shown by Gilbert [4], a k^p power law region is expected for these spectra where p is dependent on the spiral structure. The key feature of the Lundgren model is that the time-averaged energy spectrum of the structure results in an inertial range with a $k^{-5/3}$ decay of the spectrum independently of the initial condition.

In [2], computations have been performed for a particular solution of the Lundgren vortex in the form of single's spiral vortex proposed by Pullin *et al.* [5], with the stretching a , the initial lateral extension of the burst R and the Reynolds number Re taken in the experimental range.

The evolution of this particular solution has been compared with that of the experimental structure. A good agreement with the experiment has been obtained for the inertial range and for the evolution time of the structure T_v . However, in [1, 2] all the quantitative results were obtained from a time single point hot film measurement, using the delicate local Taylor hypothesis [6] in a critical condition. Moreover, since in this procedure computations of the spectra over small time records imply poor spectral resolution, a minimum time interval Δt had to be chosen for the computation of the spectra; therefore, the ability to compute instantaneous spectra was intrinsically limited.

In this paper, we present new results on this experiment using Particle Image Velocimetry (PIV) measurements that give direct access to the spatial velocity fields.

First, the characterization of the vortex burst in the spatial domain is realized. The main result is the decomposition of the velocity field as a mean velocity $\langle \mathbf{U} \rangle(\mathbf{r}, t)$ plus a perturbation field $\mathbf{u}'(\mathbf{r}, t)$. The originality of this decomposition is that the mean fields correspond to ensemble averages (and not time averages). This is why the mean velocity remains time dependent. Note also that this decomposition, based on ensemble averages, is useful for any periodical flow (e.g. wake flows).

Second, instantaneous Power Spectrum Density (PSD) are calculated directly from the velocity fields. Therefore, no use of the Taylor hypothesis is required. The obtained results confirm the temporal evolution of the instantaneous spectra, and the $k^{-5/3}$ law is recovered when instantaneous energy spectra are averaged over the whole burst lifetime.

In addition to the interest of using PIV measurements in our particular study, this paper also gives the opportunity to present for the first time a new technique to directly determine the instantaneous experimental PSD behaviour, with no need of time/space correspondence.

2. Experimental set-up

The experimental set-up is the same as the one presented in [1, 2]. A stretched vortex is generated in a low velocity hydrodynamic channel with a turbulent rate of less than 0.5%. A small step added to a laminar boundary layer profile in the bottom wall produces the initial vorticity that is strongly enhanced by the stretching produced by sucking the flow through slots on each lateral wall (figure 1). Varying the experimental parameters causes two regimes to occur: in the first one, the vortex is stable, while in the second one the vortex is experiencing periodical bursts. A laser-induced fluorescence visualization of the flow in this second regime is shown in figure 2.

We focus on this second regime which is characterized by the following experimental values: $R = 3$ cm (lateral extension of the burst), $Re = \frac{\Gamma}{\nu} = 4000$, with Γ the vortex circulation at $r = R$; a coarse estimation of the stretching is given by $a = [1-10 \text{ s}^{-1}]$ (these values are obtained from [7]). These experimental values correspond to a suction flow-rate $Q_2 = 7.5$ l/mn and a downstream flow-rate $Q_1 = 12.5$ l/mn (figure 1).

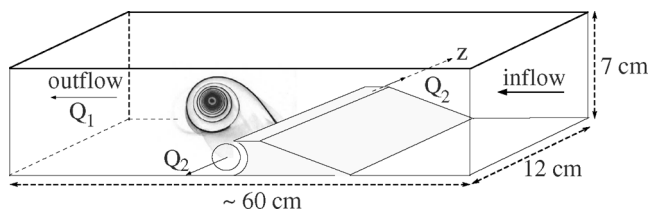


Figure 1. Experimental set-up.

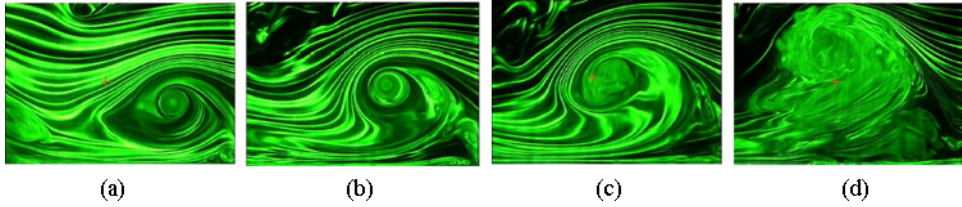


Figure 2. Laser-induced fluorescence cross-section visualization for one cycle of the flow, (a) $t = 1$ s, (b) $t = 3$ s, (c) $t = 5$ s, (d) $t = 5.5$ s. The hot film position is pictured as a red cross on the visualization. Flow goes from right to left. See also animation 1.

The velocity field of the flow is measured thanks to PIV measurements. Our PIV system is composed of a high-resolution camera (1280×1024 pixels) capturing images at a frequency of 2 Hz and a double-pulsed Nd:Yag laser delivering 12 mJ at each pulse. We use a measurement area of $5 \text{ cm} \times 4 \text{ cm}$. The interrogation window W chosen is 32×32 pixels². The spatial resolution obtained is 86×64 vectors. The PIV measurements are performed in a cross-section of the vortex at the middle of the channel [$(x, y, z = 0)$ plane] and provide therefore a measure of $\mathbf{U} = U_x \mathbf{e}_x + U_y \mathbf{e}_y$.

PIV measurements are synchronized with a hot film measurement. The beginning of the hot film acquisition is triggered by the first PIV measurement and is continuous afterwards. To achieve hot film velocity measurements with minimum flow and optical perturbations, the hot film is introduced at 45° through the lateral wall (figure 3). The probe itself is oriented at 45° so that the velocity recorded is $U = \sqrt{U_x^2 + U_y^2}$, and is shifted of 1 mm from the $z = 0$ plane to avoid any intersection with the PIV laser sheet. Finally, the hot film probe is painted with a rhodamine mixture, so that any green laser light reflected by the probe is shifted to red light and is invisible to the camera which is equipped with an optical green filter pass band.

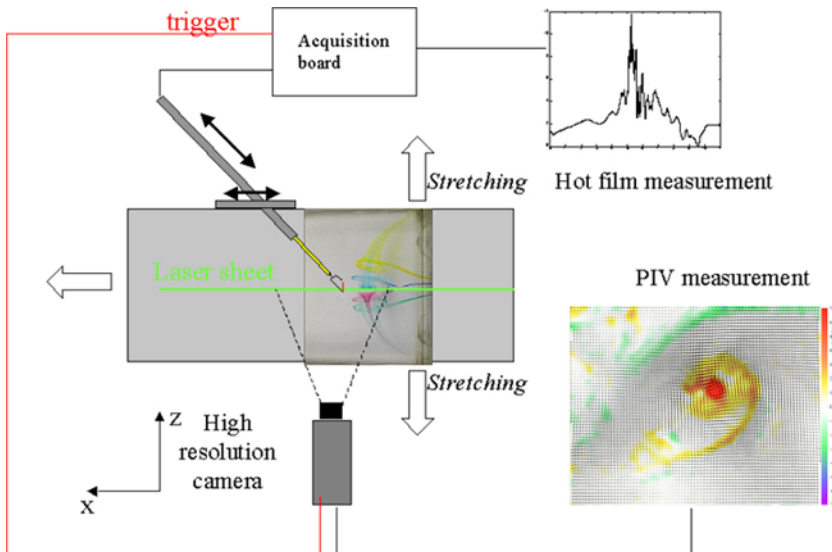


Figure 3. Experimental set-up for synchronized PIV and hot film acquisition.

3. Data processing

Let us recall the main features of our flow that motivate our data processing. We are interested in the temporal build-up of the turbulent energy cascade. Our experiment produces a turbulent burst that evolves in time, without forcing. This burst occurs periodically, allowing for ensemble averages. Here, ensemble average means average over lots of events, each taken at the same instant in each cycle.

PIV measurements give direct instantaneous velocity fields. To make possible ensemble averages at any instant of the cycle, these fields have to be time located within the cycle. To do that, we use the temporal velocity signal measured by the hot film probe (with absolute time) on which the cycles can be identified, this signal being synchronized with PIV. The treatment of the data is then as described below.

A typical velocity signal from the hot film shows the periodicity of the flow (a period of duration $T \sim 10$ s is formed of a laminar phase and a turbulent phase; see figure 4). Times t_n for the beginning of the n th cycle are determined via an *ad hoc* post-processing of this signal detailed in [2].

Simultaneously to the hot film acquisition, a large number of PIV velocity fields are recorded ($N \sim 4000$ corresponding to about 200 cycles). The acquisition time t_a of each velocity field is first rescaled using $t = t_a - t_n$, with $0 \leq t \leq T$. Hence, all velocity fields, which initially come from different cycles, are indiscriminately time located (with time t) in a unique (virtual) cycle.

With an acquisition frequency of the hot film of 400 Hz, the whole cycle $[0, T]$ is naturally divided into 4000 time intervals. To obtain about 10 fields in each interval, we should record 40 000 fields. Because we cannot do that, we use the following procedure: The time interval $[0, T]$ is divided into short sub-intervals $I_i = [t_i, t_i + \Delta t]$, with $\Delta t \ll T$ but large enough to have several velocity fields in each interval. With $\Delta t = 0.1$ s, approximately 40 velocity fields are recorded at time $t \in I_i$. These velocity fields are denoted as $\mathbf{U}_p(\mathbf{r}, t)$, with index by $p = 1, \dots, N_p \sim 40$. It is now possible to define the ensemble average at time t_i

$$\langle \mathbf{U} \rangle(\mathbf{r}, t_i) \equiv \frac{1}{N_p} \sum_p \mathbf{U}_p(\mathbf{r}, t \in I_i). \quad (1)$$

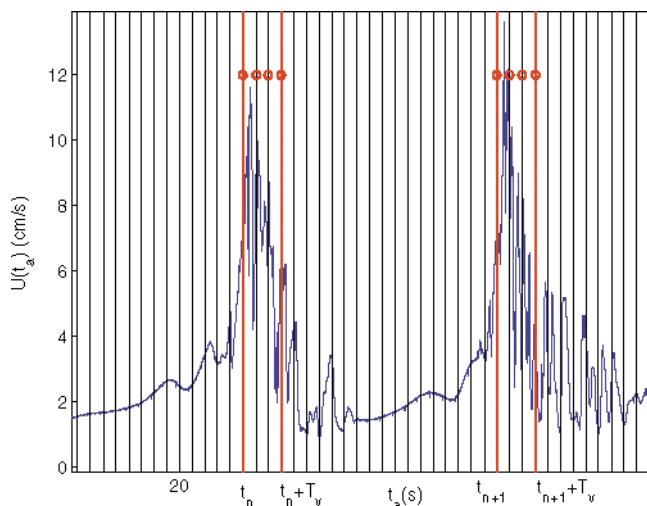


Figure 4. Example of two cycles on a typical hot film velocity signal. Times of PIV measurements are symbolized as black vertical lines; times t_n for the beginning of the turbulent parts are symbolized as red thick vertical lines.

To define the mean fields (from which fluctuation fields will be deduced), another difficulty has to be taken into account. In the time evolution of the turbulent burst (see figure 2 and animation 1), we identify a coherent structure remaining over the whole cycle. This structure is coherent in the sense that it concentrates the vorticity but also in the sense that it coherently evolves in time along a trajectory that only slightly differs from one cycle to another. This has to be opposed to the vorticity patches that randomly appear when the vortex explodes, with no coherence from one cycle to another.

We identify the mean field as the ensemble average that conserves this coherent structure field, whose centre is defined at the maximum vorticity location. Thus, even if the trajectories of this structure differ only slightly, we have to perform a recentring of the instantaneous fields over the mean trajectory before summing them as in equation (1). For $t \in I_i$, $\mathbf{R}_p(t)$ denotes the vector position of maximum vorticity of $\boldsymbol{\omega}_p \equiv \nabla \times \mathbf{U}_p$ ($\boldsymbol{\omega}_p = \omega_p \mathbf{e}_z$ is computed from the velocity signal). The mean trajectory of the coherent structure is

$$\langle \mathbf{R} \rangle(t_i) \equiv \frac{1}{N_p} \sum_p \mathbf{R}_p(t \in I_i),$$

and the spatial shift is $\delta \mathbf{r}_p \equiv \mathbf{R}_p - \langle \mathbf{R} \rangle$

The shift $\delta \mathbf{r}_p$ is determined as follows: At a first step, it is set to zero and $\langle \omega \rangle_0(\mathbf{r}, t_i)$ is calculated from equation (1) as the ensemble average without centring. The shift $\delta \mathbf{r}_p$ is then estimated as the values that maximizes the intercorrelation function $\rho(\mathbf{r}, t_i)$ between $\omega_p(\mathbf{r}, t \in I_i)$ and $\langle \omega \rangle_0(\mathbf{r}, t_i)$:

$$\begin{aligned} \rho(\mathbf{r}, t_i) &\equiv \int_S \langle \omega \rangle_0(\mathbf{r}_0, t_i) \omega_p(\mathbf{r}_0 + \mathbf{r}, t) d\mathbf{r}_0, \\ \rho(\delta \mathbf{r}_p, t_i) &= \max[\rho(\mathbf{r}, t_i)], \end{aligned} \quad (2)$$

where S is the same surface for all p values. In this definition, the shift gives the translation needed to put the coherent structure of the p^{th} field on its mean trajectory (estimated at zero order). All fields can now be centred using the change of co-ordinates $\mathbf{r} \rightarrow \mathbf{r} - \delta \mathbf{r}_p$, and the ensemble average can be taken as in equation (1). Note that we could iterate the process using $\langle \omega \rangle_0(\mathbf{r}, t_i)$ obtained after the first centring instead of $\langle \omega \rangle_1(\mathbf{r}, t_i)$. It has been checked that no significant difference occurs after the first iteration. The mean fields being defined, the decompositions

$$\begin{aligned} \mathbf{U}_p(\mathbf{r}, t \in I_i) &\equiv \langle \mathbf{U} \rangle(\mathbf{r}, t_i) + u'_p(\mathbf{r}, t), \\ \omega_p(\mathbf{r}, t \in I_i) &\equiv \langle \omega \rangle(\mathbf{r}, t_i) + \omega'_p(\mathbf{r}, t) \end{aligned} \quad (3)$$

are meaningful, with (by construction) the fluctuation fields $u'_p(\mathbf{r}, t)$, and $\omega'_p(\mathbf{r}, t)$, verifying $\langle u' \rangle(\mathbf{r}, t_i) = 0$, $\langle \omega' \rangle(\mathbf{r}, t_i) = 0$.

An example of decomposition between mean and fluctuating vorticity at $t_i = 0$ s is shown in figure 5. This decomposition clearly exhibits a fluctuation part composed of vorticity patches structures surrounding a nearly axisymmetric averaged vorticity field $\langle \omega \rangle$.

Note that, in the following, t_i and t are no more distinguished. Additionally, index p is omitted.

4. Characterization of the experimental vortex in the physical space

In order to modelize the flow as a Lundgren type vortex, the differential rotation $\Omega(r, t)$, whose relation with the mean vorticity field is detailed below, is an interesting quantity to

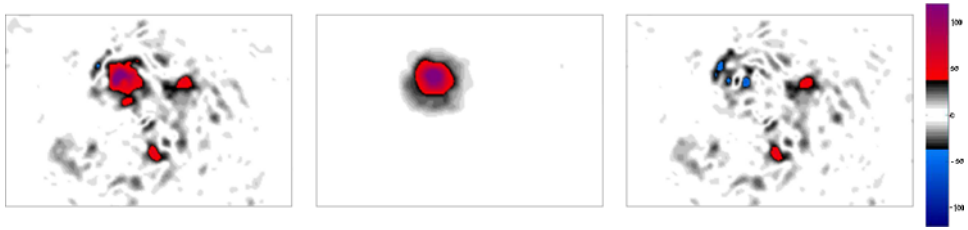


Figure 5. Examples of decomposition between mean vorticity and fluctuating vorticity at $t_i = 0$ s. From left to right: the whole vorticity field $\omega_p(\mathbf{r}, t)$, the mean vorticity field $\langle \omega \rangle(\mathbf{r}, t_i = 0)$ and the fluctuating vorticity field $\omega'_p(\mathbf{r}, t)$

be determined. Indeed, it is a key feature in Lundgren's mechanism, that, associated with stretching, enables the energy transfer towards small scales.

4.1 Definition and role of the differential rotation in the Lundgren model

Lundgren's asymptotic solution results from two keys: First, the derivation of a bi-dimensional equation for vorticity

$$\partial_t \omega + (\mathbf{U} \cdot \nabla) \omega = \nu \Delta \omega, \quad (4)$$

written in new stretched variables for time and space $t \rightarrow [e^{at} - 1]/a$, $r \rightarrow r e^{at/2}$, and for new functions $f \rightarrow e^{at} f$.

Second, the linearization of this equation is performed (valid for long time) where the velocity reduces to its zero harmonic azimuthal component (this is a—non-trivial—consequence of the hypothesis that all Fourier component of the vorticity persist for long time). Each Fourier component of the vorticity ω_n , with $\omega = \sum_n \omega_n e^{in\theta}$, follows a simple convection–diffusion equation

$$\partial_t \omega_n + in \frac{U_0}{r} \omega_n = \nu \Delta \omega_n. \quad (5)$$

With

$$\Omega \equiv \frac{U_0}{r} = \frac{1}{r^2} \int_0^r r' \omega_0 dr', \quad (6)$$

the inviscid part of the solution is written as $e^{in(\theta - \omega t)}$ (the complete solution is derived in [3] and contains this term also). This shows that the non-axisymmetric vorticity winds up into sheet like structures because of this differential rotation Ω , while the stretching (an effect which appears when we come back to a real spatial variable $r e^{-at/2}$) contracts the whole structure into closer sheets. This is also the picture of the transfer from large to smaller scales in the physical space: the scales correspond to the periodicity of the vorticity sheets that decreases when time increases. This is why Ω appears as an important parameter: combined to stretching, it ensures the process of energy transfer from large to small scales and fixes the accumulation rate of spiral turns.

The initial vorticity field $\omega(r, t = 0)$ is a free parameter in the Lundgren's model that always leads to solutions with a $k^{-5/3}$ spectrum. However, the temporal evolution of the instantaneous spectra is influenced by the initial condition that fixes Ω . It has been notably shown by Vassilicos and Pedrezetti [8] and Borgnat [9] that the rate of energy transfer is fixed by Ω .

Several forms for $\Omega(r)$ are proposed in the literature depending on the particular solution of the Lundgren vortex considered. A common class of solutions consider a Lundgren vortex in the form of a single spiral vorticity layer. For such a solution the self-induced rotation $\Omega(r)$

of the layer is generally characterized by a power law decay (r^α , $\alpha < 0$). Such solutions have been notably studied by Vassilicos and Brasseur [10] (without stretching) and Borgnat [9]. The solution of Pullin et al. [5] studied in [2] can be classified in this family of solutions, but consider a halo of opposite vorticity surrounding the vortex in order to keep zero circulation at infinity. In a two-dimensional study, Gilbert [4] has also considered shearing of vorticity patches by a power law differential rotation.

Another type of particular solution, proposed by Lundgren [11], considers a Burgers vortex core and spiral arms. In this case, $\Omega(r)$ may be dominated by the vortex core induced rotation rather than by the spiral-induced rotation. Therefore $\Omega(r)$ shows a near r^{-2} decay outward of the vortex core region.

4.2 Definition of the differential rotation for the experimental flow

We define the axisymmetric vorticity as the mean vorticity $\langle \omega \rangle$. Because $\langle \omega \rangle$ is slightly non-axisymmetric, this is done through

$$\omega_0(r, t) = \frac{1}{2\pi} \int_0^{2\pi} \langle \omega \rangle(r, \theta, t) d\theta, \quad (7)$$

from which rotation $\Omega(r, t)$ is computed

$$\Omega(r, t) = \frac{1}{r^2} \int_0^r r' \omega_0(r', t) dr' \quad (8)$$

Figures 6 and 7 show the time evolution of $\Omega(r)$ and $\omega(r)$. A monotone decrease of $\Omega(r)$ is observed for all time, a condition for the validity of Lundgren's asymptotic development (see [3]). The mean profile is characterized by a first region $0 < r < 0.2$ cm of almost solid body rotation defining the vortex core. A second region $0.5 \text{ cm} < r < 2 \text{ cm}$ is characterized by an r^α algebraic decay of the rotation Ω , where α , whose initial value is -1.6 , shows a slight increase with increasing time. This decay is significantly smoother than the near r^{-2} decay associated with the near irrotational region of the vortex in its stable state [12]. Therefore, it

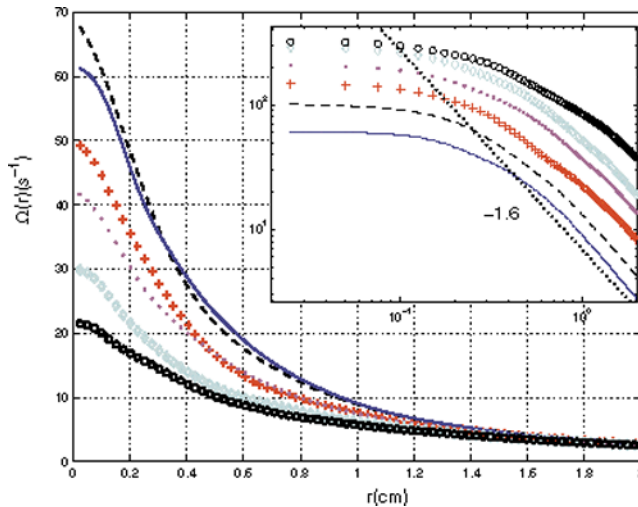


Figure 6. Evolution of differential rotation $\Omega(r, t)$, $t = 0$ s blue (—), $t = 0.2$ s black (—), $t = 0.4$ s red (+), $t = 0.6$ s magenta (●), $t = 0.8$ s cyan (◇), and $t = 1.3$ s black (○). The inset shows the same data in logarithmic co-ordinates, The curves are artificially vertically shifted for clarity.

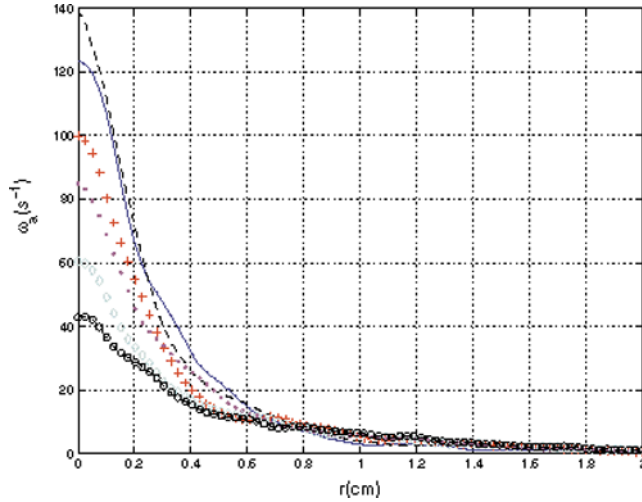


Figure 7. Evolution of the axisymmetric vorticity $\omega_0(r, t)$, $t = 0$ s blue (—), $t = 0.2$ s black (—), $t = 0.4$ s red (+), $t = 0.6$ s magenta (●), $t = 0.8$ s cyan (◊), and $t = 1.3$ s black (○).

appears that vorticity in the periphery of the vortex core gives a significant contribution to the mean rotation.

These results should provide useful material for the modelling of the experimental turbulent vortex as a Lundgren vortex solution.

5. Characterization of the vortex in the spectral space

5.1 Computations of the energy spectra from the hot film signal

An important issue of the present study is the characterization of the build-up of the turbulent energy spectrum with time. In order to characterize the temporal evolution of the burst in the spectral space, we have defined in [1, 2] quasi-instantaneous energy spectra and cumulative spectra from the hot film measurements, which provide, respectively, the quasi-instantaneous and time-integrated spectral signature of the turbulent vortex. However, two difficulties arise in the computation of these spectra from the hot film measurements.

First, the correspondence between temporal velocity fluctuations and spatial velocity fluctuations is achieved using a local Taylor hypothesis in a critical condition. Second, to keep a minimal spectral resolution, spectra are computed over a minimal time interval Δt , incompressible whatever the number of recorded cycles. In [1, 2] Δt was chosen in order to keep a constant $\Delta r = 1.5$ cm.

The use of PIV measurements overcomes these two difficulties.

5.2 Computation of the spectra from the PIV signal

Computations from PIV measurements of quantities such as energy spectra that characterizes all the scales of a turbulent flow is not usual. Indeed, the dynamical velocity range (DVR) and the dynamical spatial range (DSR) obtained from a PIV measurements are still limited. Following Adrian [13] the DVR and the DSR are estimated as follows:

- The DSR is fixed by the ratio between the physical size $Lx \times Ly$ of the velocity field and the physical size of the interrogation window $M_0 \times W$ (where M_0 is the optical magnification).
- The DVR is fixed by the ratio between the maximum resolved velocity U_{\max} and the measurement noise σ_u . This noise results from various sources: physical (dynamical and optical characteristics of the particles, characteristics of the laser sheet), specificity of the flow (out of plane motions, velocity gradients), instrumental (camera and digitalization) and can be modeled as a white noise [14].

The interrogation window W and the physical size $Lx \times Ly$ have to be chosen so that the bandpass of PIV fits the range of scales and velocities to be characterized. The optimal DVR and DSR are obtained in our experiment for $W = 32 \times 32$ pixels² and $(Lx \times Ly = 5 \text{ cm} \times 3.8 \text{ cm})$. For these values, the DSR is (0.06 cm, 5 cm) which is *a priori* sufficient to resolve the inertial range scales estimated as $0.5 \text{ cm} < r < 5 \text{ cm}$ in [1, 2].

Following Foucaut *et al.* [14], an estimation of the noise level σ_u is obtained from the comparison between the hot film energy spectrum and the PIV energy spectrum. For the values of (Lx, Ly, W) chosen, we find $\sigma_u \sim 0.1 \text{ cm s}^{-1}$. The resulting DVR (0.1 cm s^{-1} , 40 cm s^{-1}) is therefore sufficient to resolve the velocities u associated with the inertial range scales r , which can be estimated as $1 \text{ cm s}^{-1} < u < 20 \text{ cm s}^{-1}$ from hot film measurements.

The instantaneous bi-dimensional velocity PSD $e(k, t)$ writes

$$e(k, t) \equiv k \int_0^{2\pi} |\widehat{\mathbf{u}}(\mathbf{k}, t)|^2 d\theta_k, \quad (9)$$

where $k \equiv (k, \theta_k)$ in polar co-ordinates, and $\widehat{\mathbf{u}}(\mathbf{k}, t)$ is the fourier transform of $\mathbf{u}'(\mathbf{r}, t)$.

Experimentally, the energy spectra are calculated for $t = t_i$ (times t_i are defined in section 3). In equation (9), time t equals t_i on the left-hand side term and the integral on the right-hand side term is evaluated as follows: First, the Fourier transform of the fluctuation velocity fields for $t \in I_i$ is calculated (using a Hannig window), yielding to a set of N_p spectral fields $|\widehat{\mathbf{u}}(\mathbf{k}, t \in I_i)|^2$. The ensemble average $\langle |\widehat{\mathbf{u}}'|^2 \rangle(\mathbf{k}, t_i)$ is then taken over the N_p fields, as defined in equation (1). The obtained field, being defined on a Cartesian grid, is interpolated over a polar grid and integrated at each constant k radius, after which it is multiplied by k as in equation (9).

Note that the velocity PSD is also linked to the vorticity field through

$$e(k, t) = \frac{1}{k} \int_0^{2\pi} |\widehat{\omega}'(\mathbf{k}, t)|^2 d\theta_k, \quad (10)$$

and the same procedure is used to experimentally calculate $e(k, t_i)$ using the vorticity fields obtained from the velocity fields (equation (3)).

From these instantaneous spectra, the cumulative spectrum, representing the time-integrated contribution of the turbulent vortex to the spectrum, is simply defined as the time-average over instantaneous spectra

$$E^c(k, t) \equiv \int_0^t e(k, t') dt', \quad (11)$$

and is experimentally calculated through

$$E^c(k, t) = \frac{1}{i} \sum_{j=1}^i e(k, t_j). \quad (12)$$

5.3 Results

In this section, we present results obtained for the energy spectra computed from the PIV data. These results are compared with the spectra computed from the corresponding synchronized hot film measurement. For the sake of clarity, energy spectra computed from the PIV vorticity field (equation (10)) are identified with the index 1, those from the PIV velocity field (equation (9)) with the index 2, and those from the hot film with the index 3.

5.3.1 Mean energy spectra. For increasing time value, the cumulative spectrum in equations (11) and (12) is found to converge. We call T_v the time that ensures that the cumulative spectrum has converged with a desired accuracy, and we call the mean energy spectrum $E(k) \equiv E^c(k, T_v)$. Practically, it is found that the cumulative spectra calculated from PIV measurements converge in a time $T_v \simeq 2$ s, larger than the cumulative spectra calculated from the hot film acquisition (see section 5.3.3). Choosing in all cases T_v as the lifetime for the turbulent cascade build-up, we ensure

$$E_a(k) = E_a^c(k, t = 2s), \quad a = 1, 2, 3, \quad (13)$$

have converged.

The mean energy spectra computed from PIV vorticity fields [$E_1(k)$], from PIV velocity fields [$E_2(k)$], and the corresponding synchronized hot film acquisition [$E_3(k)$] are represented in figure 8. The hot film energy spectrum shows a neat Kolmogorov $k^{-5/3}$ fall-off between $k_m = 0.2 \text{ cm}^{-1}$ and $k_M = 2 \text{ cm}^{-1}$. It has been shown in [1, 2] that this inertial range is consistent with the inertial range estimation for a Lundgren energy cascade mechanism in the same (experimental) conditions.

Most of the $k^{-5/3}$ inertial range is recovered on the 2 PIV energy spectra. This result confirms both the $-5/3$ decay and the ability of PIV measurements to characterize the scales in the inertial range.

For wave numbers k in the dissipative range, a discrepancy between the PIV spectra $E_1(k)$ and the hot film spectrum $E_3(k)$ is observed. A steeper decay is observed for the energy spectrum computed from the vorticity field. This steeper decay results from a low-pass filtering related to the estimation of the vorticity field based on finite differences. A divergence between $E_1(k)$ and $E_3(k)$ is also observed in the dissipative range as a consequence of the measurement noise σ_u . Indeed, this noise brings a spurious constant contribution to the

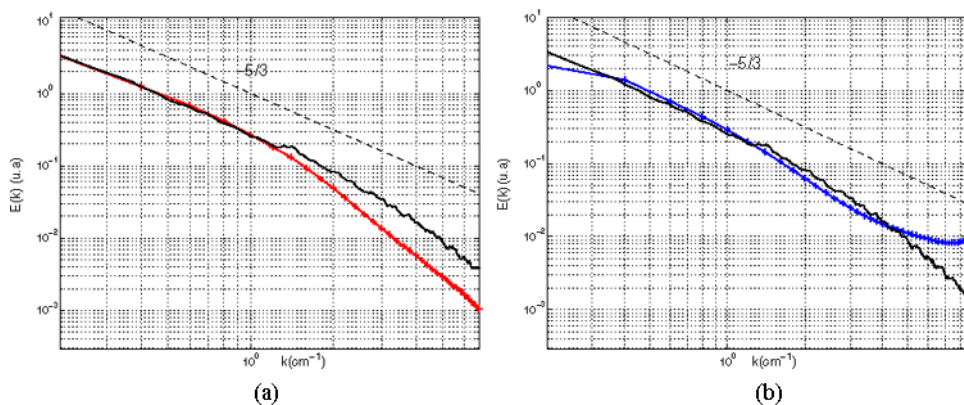


Figure 8. (a) red (+), PIV energy spectrum $E_1(k)$, obtained from the vorticity field; (–), hot film energy spectrum $E_3(k)$. (b) blue (+), PIV energy spectrum obtained from the velocity field $E_2(k)$; (–), hot film energy spectrum $E_3(k)$.

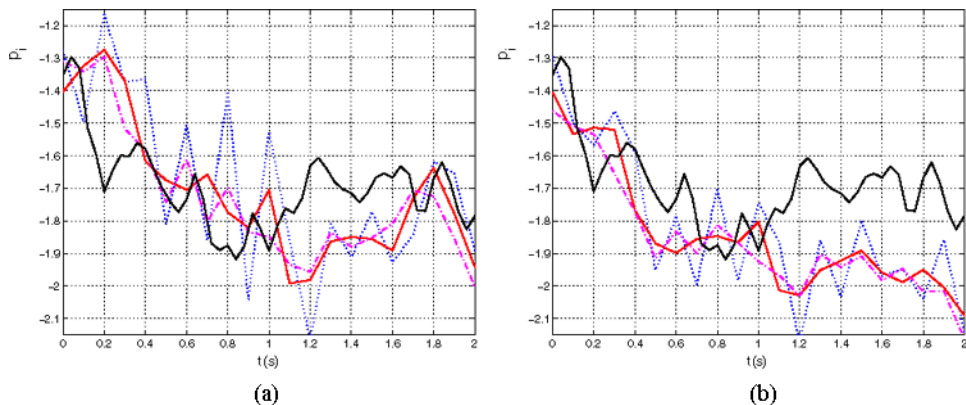


Figure 9. Comparison in the evolution of the instantaneous spectral exponent p_i computed from (a) PIV vorticity fields and from (b) velocity fields. For each plot, in blue (..) $\Delta t = 0.1$ s, in red (—), $\Delta t = 0.2$ s, in magenta (- -) $\Delta t = 0.3$ s. The spectral exponent computed from hot film (with $\Delta r = 2.5$ cm, for detail see [2]) is indicated in black (—).

spectrum that is no more negligible for the low-energy density levels associated with high wave numbers. Finally note that the first point ($k = 0.2 \text{ cm}^{-1}$) of $E_1(k)$ has a lower value than the first point of $E_3(k)$. This may result from the windowing effect; indeed, large scales of the velocity field are comparable to the window size. Such a low value at $k = 0.2 \text{ cm}^{-1}$ is not observed for the vorticity spectrum $E_2(k)$, because vorticity scales are much smaller than the window size.

5.3.2 Instantaneous energy spectra. The evolution of the instantaneous energy spectra is characterized by the evolution of the spectral exponent p_i computed over the inertial range. This evolution is compared for the PIV spectra and for the hot film spectra in figure 9. To ensure robustness of the spectra, the spectral slopes $p_{i,1}$, $p_{i,2}$ are computed for several values of the time interval Δt between each time t_i (defined in section 3), ranging from 0.1 to 0.3 s. A general evolution trend from -1 to -2 of the spectral slope is observed for both PIV and hot film data. This confirms previous results obtained from hot film measurements in [1, 2] and the ability of the PIV phase-averaged measurements to resolve the dynamic evolution of the burst.

In [2], the temporal evolution of the instantaneous spectra, from -1 to -2 has to be contrasted with the temporal evolution (from -2 to -1) of the classical single spiral structure, often exhibited when Lundgren’s model is advocated. We had suggested in [2] that the -1 spectral exponent, which results from the spatial vorticity distribution (at $t = 0$), could be explained by an initial spatial vorticity distribution in the form of vorticity patches randomly ejected by the coherent structure when it explodes, rather than the vorticity sheet that leads in the -2 behaviour in [5, 11]. Images of the fluctuating vorticity field for initial time $t_i = 0$ s, one of which is shown in figure 5, reinforce this hypothesis.

5.3.3 Cumulative energy spectra. The evolution of the cumulative spectra computed from PIV velocity and vorticity fields [$E_{1,2}^c(k, t)$] and from the hot film data [$E_3^c(k, t)$] is represented in figure 10. In each case, an evolution from -1 to $-5/3$ is observed. This confirms that the $-5/3$ law only emerges from a time averaging of the instantaneous spectra as in the Lundgren vortex model.

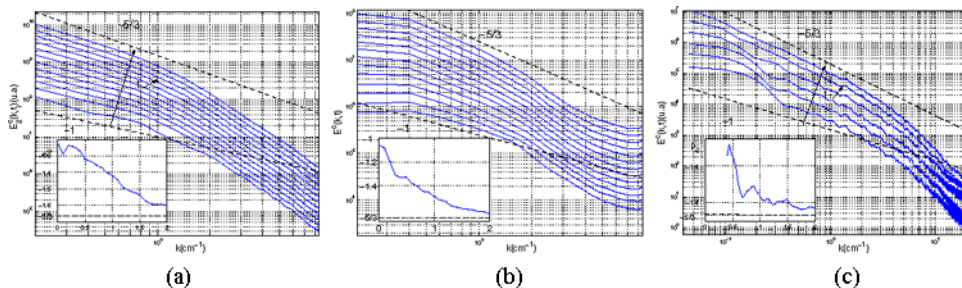


Figure 10. Cumulative spectra $E^c(k, t)$ calculated (a) from the PIV vorticity field $E_1^c(k, t)$, (b) from the PIV velocity field $E_2^c(k, t)$ and (c) from the hot film signal $E_3^c(k, t)$; the spectra are artificially vertically shifted. In each case, an inset shows the evolution of the spectral exponent.

The time needed for the turbulent cascade build-up is around $T_v \simeq 2$ s. This time is in agreement with Lundgren's spiral lifetime estimated in [5, 2] as $\tau_v = C(R^2/4\nu)Re^{-2/3}$, where C is a constant (obtained in numerical computations equal to 10) and τ_v is a stretched time variable (see section 4.1). Considering the coarse estimation of the stretching given in section 2, this yields to $0.5 \text{ s} \leq T_v \leq 2.5 \text{ s}$. Estimation of T_v appears to be slightly different when considering the cumulative spectra computed from the PIV data ($T_v \simeq 2$ s) and when considering the spectra computed from the hot film data (the value is close to 1.5 s, as it was obtained previously in [2] using other set of data). It should be pointed out that cumulative spectra calculated from the hot film acquisition are computed from a time-increasing window: This is because the mean velocity decreases in time so that the time/space correspondence $\delta r = \langle U \rangle(t)\delta t$ imposes an increasing δt value to keep a constant spectral range. Therefore, the temporal resolution of $E_3^c(k, t)$ decreases with increasing time and can affect the spectral exponents. Such an effect does not affect the exponents of the cumulative spectra calculated from PIV measurements, since, by construction, they keep the same spectral resolution at any time with no need of time/space correspondence.

6. Conclusion

Using phase-averaged PIV measurements, the transition to turbulence of our isolated structure has been characterized in both physical and spectral spaces.

In the physical space, thanks to ensemble averages, velocity fields have been decomposed into mean and fluctuating velocity fields. From the mean velocity field, the evolution of the differential rotation Ω has been characterized. It has been notably shown that it is a decreasing function of r , a condition in the derivation of the asymptotic solution of Lundgren. This suggests that our experimental conditions are favourable to permit that our burst indeed follows a Lundgren's mechanism of energy transfer.

In the spectral space, the use of PIV measurements overcomes difficulties encountered in the calculation of instantaneous energy spectra from the hot film data, results that have been previously presented [1, 2]. The -1 to -2 transition of the instantaneous spectral slopes is confirmed, as well as the $k^{-5/3}$ law obtained when averaging the spectra over the whole burst lifetime.

A perspective to this work is the modelling of the experimental flow as a Lundgren vortex. PIV data should provide helpful material in this perspective. Also, on the basis of the PIV data, the characterization of the energy transfers and associated intermittency should be achievable.

References

- [1] Cuypers, Y., Maurel, A. and Petitjeans, P., 2003, Vortex burst as a source of turbulence. *Phys. Rev. Lett.*, **91**, 194502.
- [2] Cuypers, Y., Maurel, A. and Petitjeans, P., 2004, Comparison between an experimental turbulent vortex and the Lundgren vortex. *J. Turbulence*, **5**, 1–22.
- [3] Lundgren, T.S., 1982, Strained spiral vortex model for turbulent fine structures. *Phys. Fluids*, **25**, 2193.
- [4] Gilbert, A.D., 1988, Spiral structures and spectra in two-dimensional turbulence. *J. Fluid Mech.*, **193**, 475.
- [5] Pullin, D.I., Buntine, J.D. and Saffman, P.G., 1994, On the spectrum of a stretched spiral vortex. *Phys. Fluids*, **6**, 3010.
- [6] Pinton, J.F. and Labbe, R., 1994, Correction to the Taylor hypothesis in swirling flows. *J. Phys. II*, **4**, 1461.
- [7] Manneville, S., Robres, J.H., Maurel, A., Petitjeans, P. and Fink, M., 1999, Vortex dynamics investigation using an acoustic technique. *Phys. Fluids*, **11**(11), 3380–3389.
- [8] Vassilicos, J.C. and Pedrizzetti, G., 2000, Interscale transfer in two dimensional compact vortices. *J. Fluid Mech.*, **406**, 109.
- [9] Borgnat, P., 2002, Modèles et outils pour les invariances d'échelles brisées Thèse de l'Ecole Normale Supérieure de Lyon.
- [10] Vassilicos, J.C. and Brasseur, J.G., 1996, Self-similar spiral flow structure in low Reynolds number isotropic and decaying turbulence. *Phys. Rev.*, **E54**(1), 467.
- [11] Lundgren, T.S., 1993, A small-scale turbulence model. *Phys. Fluids*, **A5**, 1472.
- [12] Rossi, M., Bottausci, F., Maurel, A. and Petitjeans, P., 2004, A non uniform stretched vortex. *Phys. Rev. Lett.*, **92**, 54504.
- [13] Adrian, R.J., 1997, Dynamic ranges of velocity and spatial resolution of particle image velocimetry. *Meas. Sci. Technol.*, **8**, 1393.
- [14] Foucaut, J.M., Carlier, J. and Stanislas, M., 2004, PIV optimization for the study of turbulent flow using spectral analysis. *Meas. Sci. Technol.*, **15**, 1046.